SANDIA REPORT

SAND2014-18590
Unlimited Release
Printed September 2014

Peridynamic Model for Fatigue Cracking

Stewart A. Silling

Abe Askari

Prepared by
Sandia National Laboratories
Albuquerque, New Mexico 87185 and Livermore, California 94550

Sandia National Laboratories is a multi-program laboratory managed and operated by Sandia Corporation, a wholly owned subsidiary of Lockheed Martin Corporation, for the U.S. Department of Energy's National Nuclear Security Administration under contract DE-AC04-94AL85000.

Sandia National Laboratories

Issued by Sandia National Laboratories, operated for the United States Department of Energy by Sandia Corporation.

Available to DOE and DOE contractors from
U.S. Department of Energy
Office of Scientific and Technical Information
P.O. Box 62
Oak Ridge, TN 37831

Telephone: (865) 576-8401
Facsimile: (865) 576-5728
E-Mail: reports@adonis.osti.gov
Online ordering: http://www.osti.gov/bridge

Available to the public from
U.S. Department of Commerce
National Technical Information Service
5285 Port Royal Rd
Springfield, VA 22161

Telephone: (800) 553-6847
Facsimile: (703) 605-6900
E-Mail: orders@ntis.fedworld.gov
Online ordering: http://www.ntis.gov/help/ordermethods.asp?loc=7-4-0#online

SAND2014-18590
Unlimited Release
Printed September 2014

Peridynamic Model for Fatigue Cracking

Stewart A. Silling
Multiscale Science Department
Sandia National Laboratories
Albuquerque, NM 87185-1322

Abe Askari
Propulsion System Engineering
The Boeing Company
Seattle, WA

Abstract

The peridynamic theory is an extension of traditional solid mechanics in which the field equations can be applied on discontinuities, such as growing cracks. This paper proposes a bond damage model within peridynamics to treat the nucleation and growth of cracks due to cyclic loading. Bond damage occurs according to the evolution of a variable called the "remaining life" of each bond that changes over time according to the cyclic strain in the bond. It is shown that the model reproduces the main features of S-N data for typical materials and also reproduces the Paris law for fatigue crack growth. Extensions of the model account for the effects of loading spectrum, fatigue limit, and variable load ratio. A three-dimensional example illustrates the nucleation and growth of a helical fatigue crack in the torsion of an aluminum alloy rod.

Acknowledgment

This work was sponsored by The Boeing Company through CRADA No. SC02/01651.

Contents

Figures

1 Introduction

The ability to understand the process of fatigue cracking in complex structures and heterogeneous materials depends on the ability to model damage nucleation and the growth of curved, three-dimensional cracks under general loading conditions. The peridynamic model [26], by virtue of treating discontinuities with the same mathematical equations as points where the deformation is continuous, potentially avoids some of the difficulties of traditional computational methods in treating complex patterns of fatigue crack growth. Because peridynamics does not assume a pre-existing crack, it also potentially offers a way to model the nucleation and growth phases of damage consistently. This paper presents an attempt to apply the peridynamic approach to the nucleation and growth of fatigue cracks.

Most modern continuum treatments of the growth of a crack under cyclic loading are derived from the Paris law [21]. Various corrections have been proposed for this law, while retaining the basic idea that the cyclic change in stress concentration factor at the crack tip is the driving force, as discussed by Pugno *et al.* [22] and the references contained therein. A review of earlier theories is provided by Erdogan [7].

In engineering, analysis of resistance of structures to fatigue largely relies on the extrapolation of empirical data derived from geometrically simple specimens to the more complex cyclic stress field that the structure experiences. The empirical data are usually based on cyclic uniaxial states of stress compiled into S-N or ϵ-N curves. By applying these curves to stress states in structures with suitable corrections for stress concentrations due to notches and other factors, engineers can reliably design against fatigue failure (see, for example, [3]). A number of computational tools are available to apply this type of methodology to mechanical design (for example, MSC Fatigue [17]).

Other computational approaches to fatigue crack growth include that of McClung and Sehitoglu [12, 13], who used a node release method to advance the crack in a two-dimensional model and investigated the importance of mesh refinement ahead of the crack. Moës, Gravouil, and Belytschko [15, 16] and Sukumar, Chopp, and Moran [34] applied XFEM to three-dimensional fatigue crack growth. Bordas and Moran [2] describe modeling of fatigue in complex structures, using the standard Paris law, in an enriched element formulation in the EDS-PLM/I-DEAS commercial finite element code. Shi *et al.* and Shi, Chopp, Lua, Sukumar, and Belytschko [25, 24] implemented a fatigue model using XFEM in Abaqus using a modified Paris law expression. De-Adrés, Perez, and Ortiz [4] and Nguyen, Repetto, Ortiz, and Radovitzky [18] applied a cohesive element approach to fatigue crack growth, including short cracks and the effect of overload, in two dimensions. Much effort has been devoted to investigating the role of crack closure in fatigue crack growth in metals [6]; see [23] for a recent summary.

In spite of the century-old history of research on fatigue and the valuable software tools that are available to the engineer, fatigue has not been treated as a full participant within the scope continuum mechanical theory. The available models for fatigue crack nucleation (a term we use synonymously with initiation) apply some supplemental criterion that "watches"

a stress field that is computed under the assumption of continuous deformation, but is essentially a bystander in the actual computation. There has previously no way to treat the actual process of the emergence of a discontinuity due to cyclic loading within the field equations of continuum mechanics. This is not surprising, due to the well-known inapplicability of the partial differential equations of continuum mechanics on an evolving discontinuity.

The peridynamic equations, because they do not involve partial derivatives of the deformation with respect to the spatial coordinates, potentially offer a way to treat the details of fatigue crack nucleation and growth as part of a consistent mathematical description of a boundary value problem, without supplemental relations dictating crack growth. The material model, if a suitable damage law can be specified, results in accumulation of damage leading to the possible emergence of discontinuities such as cracks. The purpose of the present work is to propose and demonstrate such a material model.

2 Summary of the peridynamic theory

The peridynamic theory is an extension of the standard mathematical theory of solid mechanics that is compatible with the discontinuous nature of cracks. In contrast to the PDEs of the standard theory, which cannot be applied directly on a growing crack, the peridynamic theory uses integro-differential equations that do not involve the spatial derivatives of the deformation. The field equations therefore apply on a crack. The peridynamic model was introduced in the year 2000 [26] and has undergone extensive expansion and improvement since then. The review article [31] and the book by Madenci and Oterkus [10] contain up-to-date summaries of the theory.

The equation of motion in the peridynamic model takes the form

$$\rho(\mathbf{x})\ddot{\mathbf{y}}(\mathbf{x},t) = \int_{\mathcal{H}_{\mathbf{x}}} \mathbf{f}(\mathbf{x}',\mathbf{x},t)\, dV_{\mathbf{x}'} + \mathbf{b}(\mathbf{x},t), \qquad \forall \mathbf{x} \in \mathcal{B},\ t \geq 0 \tag{1}$$

where $\mathbf{y}$ is the deformation map, $\mathbf{x}$ is a material point in the reference configuration of a body $\mathcal{B}$, ρ is the density field, and $\mathbf{b}$ is the prescribed external body force density. The spherical neighborhood $\mathcal{H}_{\mathbf{x}} \subset \mathcal{B}$ centered at $\mathbf{x}$, but excluding $\mathbf{x}$, is called the *family* of $\mathbf{x}$:

$$\mathcal{H}_{\mathbf{x}} = \left\{ \mathbf{x}' \in \mathcal{B} \;\middle|\; 0 < |\mathbf{x}' - \mathbf{x}| \leq \delta \right\}.$$

The radius of the neighborhood δ is called the *horizon*, which may be finite or infinite and may be thought of as a material property. The vector field $\mathbf{f}$ is the *pairwise bond force density*, which depends on the deformation through the constitutive model. Since the integral in (1) sums up forces on $\mathbf{x}$ from all of its neighbors, the peridynamic model can be thought of as a "continuum version of molecular dynamics."

The vector in the reference configuration defined by

$$\boldsymbol{\xi} = \mathbf{x}' - \mathbf{x}, \qquad \mathbf{x}' \in \mathcal{H}_{\mathbf{x}}$$

is called a *bond*. The constitutive model in the peridynamic theory prescribes the pairwise force density $\mathbf{f}$ in each bond. This pairwise force density consists of two parts that are determined by application of the constitutive model at $\mathbf{x}$ and $\mathbf{x}'$:

$$\mathbf{f}(\mathbf{x}',\mathbf{x},t) = \mathbf{t}(\mathbf{x}',\mathbf{x},t) - \mathbf{t}(\mathbf{x},\mathbf{x}',t)$$

where the two terms on the right hand side contain the contributions from $\mathcal{H}_{\mathbf{x}}$ and $\mathcal{H}_{\mathbf{x}'}$ respectively. To express the contribution from the deformation of $\mathcal{H}_{\mathbf{x}}$, we write

$$\mathbf{t}(\mathbf{x}',\mathbf{x},t) = \underline{\mathbf{T}}[\mathbf{x}]\langle \mathbf{x}' - \mathbf{x} \rangle$$

where $\underline{\mathbf{T}}[\mathbf{x}]$ is a function called the *force state* at $\mathbf{x}$ that maps any bond $\mathbf{x}' - \mathbf{x}$ to the corresponding force density vector in the bond. The force state is an example of a *peridynamic state*, which is simply a function defined on a family.

The basic kinematical quantity for purposes of constitutive modeling is the *deformation state*, whose value for any bond is the deformed image of the bond:

$$\underline{\mathbf{Y}}[\mathbf{x}]\langle \mathbf{x}' - \mathbf{x} \rangle = \mathbf{y}(\mathbf{x}', t) - \mathbf{y}(\mathbf{x}, t).$$

A constitutive model $\underline{\hat{\mathbf{T}}}$ is a state-valued function of a state:

$$\underline{\mathbf{T}} = \underline{\hat{\mathbf{T}}}(\underline{\mathbf{Y}}).$$

The structure of such a constitutitive model is analogous to a tensor valued function of a tensor in the standard theory, that is, $\boldsymbol{\sigma} = \hat{\boldsymbol{\sigma}}(\mathbf{F})$, where $\mathbf{F} = \partial \mathbf{y}/\partial \mathbf{x}$.

A constitutively linear elastic isotropic solid may be modeled as follows. For a given bond $\boldsymbol{\xi}$, define the bond direction by

$$\underline{\mathbf{M}}\langle \boldsymbol{\xi} \rangle = \frac{\boldsymbol{\xi}}{|\boldsymbol{\xi}|}.$$

Let $\underline{\omega}$ be a weighting function defined on the family, and let a normalization constant m be defined by

$$m = \int_{\mathcal{H}} \underline{\omega}\langle \boldsymbol{\xi} \rangle |\boldsymbol{\xi}|^2 \, dV_{\boldsymbol{\xi}}.$$

For any deformation state $\underline{\mathbf{Y}}$, define the *extension state* by

$$\underline{e}\langle \boldsymbol{\xi} \rangle = |\underline{\mathbf{Y}}\langle \boldsymbol{\xi} \rangle| - |\boldsymbol{\xi}| \tag{2}$$

which represents the change in length of the bond $\boldsymbol{\xi}$ under the deformation. Let the nonlocal *dilatation* be defined by

$$\theta = \frac{3}{m} \int_{\mathcal{H}} \underline{\omega}\langle \boldsymbol{\xi} \rangle |\boldsymbol{\xi}| \, \underline{e}\langle \boldsymbol{\xi} \rangle \, dV_{\boldsymbol{\xi}}.$$

This nonlocal dilatation has the same value as the dilatation in the standard (local) theory (that is, $\theta = \text{Tr}\, \epsilon$, where ϵ is the linearized strain tensor) for small, homogeneous deformations of a body. Let k be the bulk modulus and let μ be the shear modulus for the isotropic elastic solid. Then the force state is given by

$$\underline{\mathbf{T}}\langle \boldsymbol{\xi} \rangle = \frac{\underline{\omega}\langle \boldsymbol{\xi} \rangle \underline{\mathbf{M}}\langle \boldsymbol{\xi} \rangle}{m} \left[3k\theta |\boldsymbol{\xi}| + 15\mu \left(\underline{e}\langle \boldsymbol{\xi} \rangle - \frac{\theta |\boldsymbol{\xi}|}{3} \right) \right]. \tag{3}$$

The quantity that multiplies 15μ in this expression represents the deviatoric part of the deformation, that is, the extension state after the volume change is subtracted off. See [30] for further details of this model, which is called the *linear peridynamic solid* (LPS) model. Unfortunately, this name is slightly misleading because, unlike a constitutive model in the fully linearized peridynamic theory [27], the LPS model uses nonlinear kinematics (as may be seen in (2)).

Damage in peridynamics is usually modeled by irreversible *bond breakage*. After a bond breaks according to some criterion, it no longer sustains any force density. Many types of

bond breakage criteria are available. The simplest criterion is that a bond $\boldsymbol{\xi}$ breaks when its *bond strain*, defined by

$$s = \frac{e\langle \boldsymbol{\xi} \rangle}{|\boldsymbol{\xi}|}$$

exceeds some critical threshhold value s_*. This critical bond strain may vary according to position, bond length, bond direction, time, temperature, or other conditions. The fatigue model described in this paper consists of a particular bond failure criterion that does not explicitly involve a critical bond strain. Instead, each bond is characterized by a history variable that characterizes accumulated damage over many loading cycles.

In practice, the failure of one bond in a peridynamic body tends to increase the elongation of neighboring bonds, making it more likely that they too will break. This leads to progressive failure. The failures tend to organize themselves into two-dimensional surfaces that represent cracks. Bonds in many different directions contribute to crack growth, not just those bonds that are normal to the crack surface (Figure 1). Crack nucleation and growth occur spontanteously and autonomously, that is, without reference to any supplemental equations dictating these phenomena. In particular, the peridynamic approach to crack growth does not use the stress intensity factor K, which plays a fundamental role in linear elastic fracture mechanics (LEFM). (However, K will be used later in this paper for purposes of calibrating the peridynamic fatigue model with LEFM data.) The critical strain for bond breakage under non-cyclic loading of a brittle solid can be related to the critical energy release rate [28].

At a given material point $\mathbf{x}$, it is convenient to express bond damage in $\mathcal{H}_{\mathbf{x}}$ by the *damage state* $\underline{\phi}$ defined by

$$\underline{\phi}\langle \boldsymbol{\xi} \rangle = \begin{cases} 1 & \text{if } \boldsymbol{\xi} \text{ is broken,} \\ 0 & \text{otherwise,} \end{cases}$$

where $\boldsymbol{\xi}$ is any bond in the family. Properties of the damage state, including some aspects of a thermodynamic treatment, may be found in [31]. To characterize the total amount of damage at $\mathbf{x}$, define the *net damage* by

$$\phi(\mathbf{x}) = \frac{\int_{\mathcal{H}_{\mathbf{x}}} \underline{\phi}\langle \boldsymbol{\xi} \rangle \, dV_{\boldsymbol{\xi}}}{\int_{\mathcal{H}_{\mathbf{x}}} dV_{\boldsymbol{\xi}}}. \tag{4}$$

The net damage expresses the ratio of the total number of broken bonds to the initial number of bonds in a family.

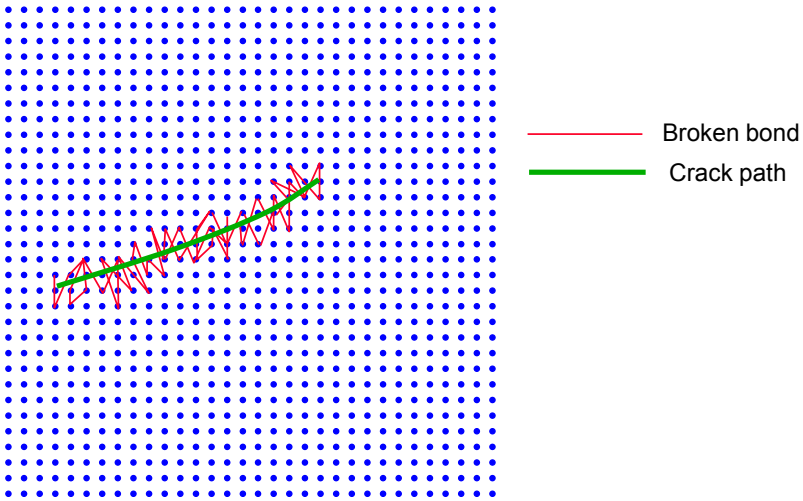

Figure 1. Crack growth in a peridynamic solid is determined by damage to bonds in many directions.

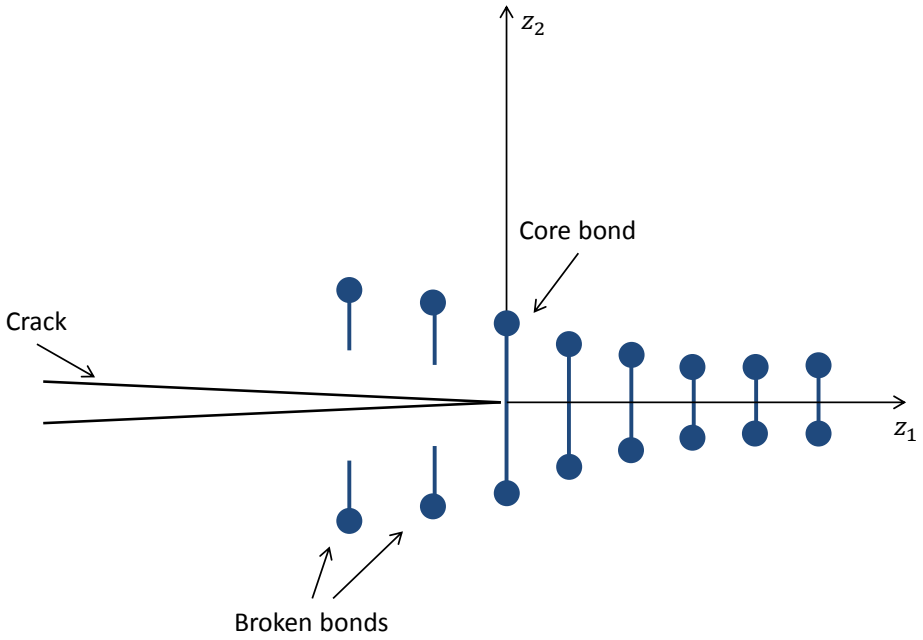

Figure 2. Schematic of bonds near a crack tip. The core bond has the largest strain. Only bonds oriented normal to the crack are shown.

3 Structure of a crack tip deformation field

Suppose we look closely at the vicinity of a mode-I crack tip in a linear elastic solid and vary the remote loading, while holding the bond damage fixed everywhere. Assume there is some bond near the crack tip whose bond strain is greater than all the others. This bond will be called the *core bond* (Figure 2). Denote its strain by s_{core}. Assuming linear behavior of the material (still holding damage fixed), s_{core} must be proportional to the stress intensity factor K that characterizes a given loading on the body, because both quantities measure the extent of deformation close to the crack tip. Also, for a given K and a given value of the Poisson ratio ν, s_{core} must be inversely proportional to the Young's modulus E, since it measures a type of strain.

A stronger statement relating s_{core} to K can be made based on a dimensional argument.

Assuming the material model is LPS, the only length scale in the peridynamic model is the horizon δ. (Other material models could contain additional length scales.) The dimensions of K, E, δ, and s_{core} are given by

$$[K] = \frac{F}{\ell^{3/2}}, \qquad [E] = \frac{F}{\ell^2}, \qquad [\delta] = \ell, \qquad [s_{\text{core}}] = 1.$$

Since there is only one way to obtain a dimensionless combination of the first three of these, and since the material response is linear, it follows that

$$s_{\text{core}}(\delta) = \hat{s}_{\text{core}} \, \frac{K}{E\sqrt{\delta}} \tag{5}$$

where $\hat{s}_{\text{core}}$ is a dimensionless parameter independent of E, K, and δ (it could depend on the Poisson ratio). By similar reasoning, for a mode-I crack tip, there must be a coordinate system $\{z_1, z_2\}$ and a function $\hat{f}$, independent of loading, such that

$$s(z_1', z_2', z_1, z_2) = s_{\text{core}}(\delta) \, \hat{f}\left(\frac{z_1'}{\delta}, \frac{z_2'}{\delta}, \frac{z_1}{\delta}, \frac{z_2}{\delta}\right) \tag{6}$$

for any two points (z_1, z_2) and (z_1', z_2') sufficiently near the origin, with $\hat{f}(0,0,0,0) = 1$.

Restricting (6) to bonds along the axis of the mode-I crack that are normal and symmetric relative to the crack, and setting $z = z_1$, we can simplify the notation and write

$$s(z) = s_{\text{core}}(\delta) \, \hat{f}\left(\frac{z}{\delta}\right), \qquad \hat{f}(0) = 1. \tag{7}$$

The loading, material properties, and length scale δ are contained in the single term $s_{\text{core}}(\delta)$, so that K and E, which are not used directly in the peridynamic model, do not appear in (7) explicitly. Sufficiently far from the crack, where $z \gg \delta$, the peridynamic bond strain field must approach the LEFM strain field. Thus, from LEFM,

$$s(z) \sim \frac{K}{E\sqrt{2\pi z}} \qquad \text{as } z \to \infty. \tag{8}$$

Combining (5), (7), and (8) leads to

$$\hat{f}\left(\frac{z}{\delta}\right) \sim \frac{1}{\hat{s}_{\text{core}}\sqrt{2\pi z/\delta}} \qquad \text{as } z \to \infty. \tag{9}$$

Illustrating the scaling results in (5), (7), and (9), the bond strain field for a few values of horizon are shown in Figure 3. A key feature is that the core strain decreases as the horizon increases, but far from the crack tip, all the curves merge together. In the limit $\delta \to 0$, the peridynamic strain field becomes more and more sharply peaked and tends toward the LEFM result. The scaling results obtained in this section will be used later to see how the parameters in the fatigue model vary as δ is changed.

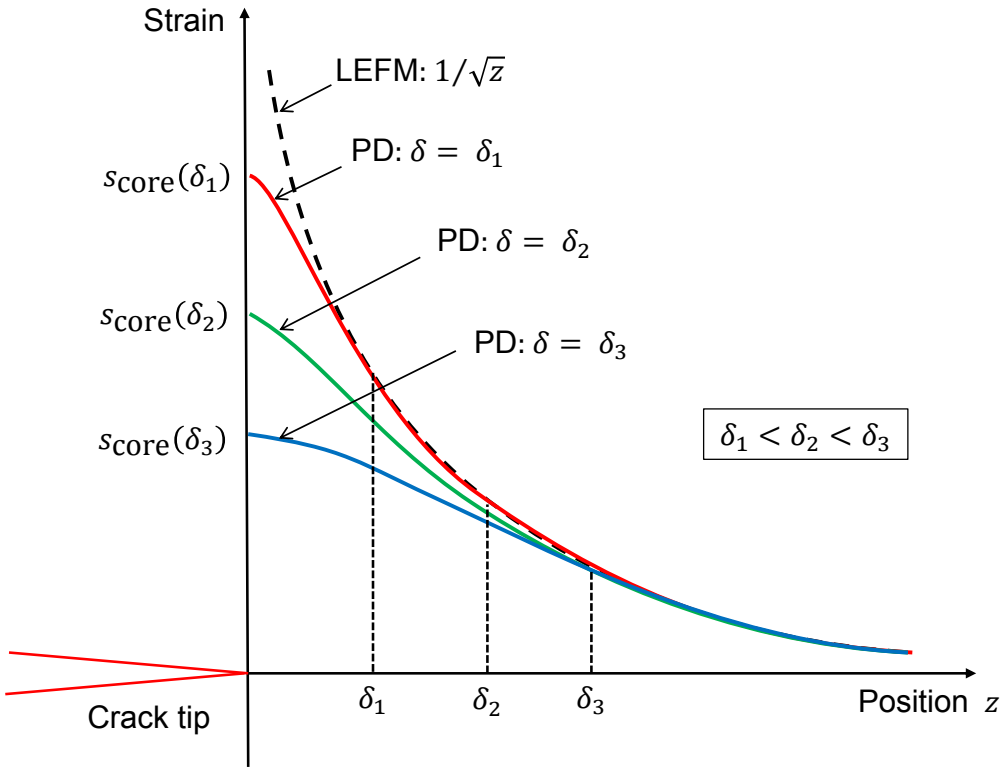

Figure 3. Bond strain ahead of a crack for three peridynamic (PD) models with varying horizon δ. All three approach the LEFM solution as distance from the crack tip increases.

4 Fatigue model

Stouffer and Williams [33], extending the work of Liu and Iino [9] and of Majumdar and Morrow [11], proposed a model in which "fatigue elements" in front of a growing crack accumulate damage according to the cyclic strain they undergo. In the present work, this general concept is applied to peridynamics bonds.

A peridynamic fatigue model has been proposed by Oterkus, Guven, and Madenci [19] that applies to the growth phase of a crack, but, as stated by these authors, not the nucleation phase. This model is formulated within the bond-based peridynamic theory, in which the force density in each bond is independent of the other bonds. This fatigue model works by degrading the critical bond strain for breakage in each bond over time, according to the prevailing cyclic loading in the bond, and it accounts for permanent strain in the bonds.

In contrast, the present work proposes a peridynamic damage model that does not explicitly involve a critical bond strain for damage. Instead, each bond is characterized by a damage variable called the "remaining life" that evolves over time, as described below. The present model is not restricted to bond-based material models, and it applies to both the nucleation and growth phases (using different choices of the parameters).

Assume that a peridynamic solid undergoes loading that cycles between two extremes, denoted + and −. Let $\mathbf{x}$ be a point in the body. For a given bond $\boldsymbol{\xi}$ in the family of $\mathbf{x}$, let the bond strains at the two extremes be defined by

$$s^+ = \frac{|\underline{\mathbf{Y}}^+\langle\boldsymbol{\xi}\rangle| - |\boldsymbol{\xi}|}{|\boldsymbol{\xi}|}, \qquad s^- = \frac{|\underline{\mathbf{Y}}^-\langle\boldsymbol{\xi}\rangle| - |\boldsymbol{\xi}|}{|\boldsymbol{\xi}|},$$

in other words the change in bond length divided by initial length. Define the *cyclic bond strain* at $\boldsymbol{\xi}$ by

$$\varepsilon = |s^+ - s^-|. \tag{10}$$

For a given $\mathbf{x}$ and $\boldsymbol{\xi}$, the quantities s^+, s^-, and ε can all depend on the cycle number N, because of the evolution of fatigue damage and other material properties. (As a fatigue crack grows closer to the bond, we expect ε to increase.)

The peridynamic fatigue model proposed here identifies with each bond $\boldsymbol{\xi}$ connected to any point $\mathbf{x}$ a *remaining life* $\lambda(\mathbf{x}, \boldsymbol{\xi}, N)$. The remaining life evolves as the loading cycle N increases according to the following relation (the $\mathbf{x}$ and $\boldsymbol{\xi}$ arguments will be omitted for simplicity):

$$\lambda(0) = 1, \qquad \frac{d\lambda}{dN}(N) = -A\varepsilon^m \tag{11}$$

where ε is the current cyclic strain in the bond, A is a positive parameter and m is a positive constant exponent. (Following the usual practice, N is treated as a real number rather than an integer.) The bond breaks irreversibly at the earliest loading cycle N such that

$$\lambda(N) \le 0. \tag{12}$$

The values of A and m in general are chosen differently according to whether a bond is in the nucleation or growth phase, as described in the next sections.

4.1 Phase I: Nucleation

Prior to the emergence of a fatigue crack, each bond $\boldsymbol{\xi}$ is in the nucleation phase of the fatigue process. In this case, the parameters A and m in (11) are set to

$$A = A_1, \qquad m = m_1 \tag{13}$$

where A_1 and m_1 are positive constants that are calibrated for the nucleation phase in a real material as described below.

Each bond in the body undergoes some cyclic strain $\varepsilon(\mathbf{x}, \boldsymbol{\xi})$. To calibrate A_1 and m_1 with experimental data, assume that the cyclic strain in each bond is independent of N. Consider the bond $\boldsymbol{\xi}_1$ connected to some point $\mathbf{x}_1$ such that this bond has the largest cyclic bond strain in the body, and call its cyclic bond strain ε_1. Since A_1 and m_1 are independent of position, and since $m_1 > 0$, this $\boldsymbol{\xi}_1$ is the bond at which damage will first nucleate. Let $\lambda_1(N)$ denote the remaining life of this bond and recall from (11) that $\lambda_1(0) = 1$. Now compute the cycle N_1 at which the bond breaks. Integrating the second of (11) over N leads to

$$A_1 {\varepsilon_1}^{m_1} N_1 = 1,$$

hence nucleation occurs when

$$N_1 = \frac{1}{A_1 {\varepsilon_1}^{m_1}}. \tag{14}$$

Here, the assumption that ε_1 is independent of N in the nucleation phase was used. The expression (14) is plotted in Figure 4, which is essentially an S-N curve in terms of strain rather than stress. The parameters A_1 and m_1 are therefore easily obtained from S-N test data for a material as indicated in the figure.

4.2 Phase II: Crack growth

To apply the peridynamic model to fatigue crack growth, (11) with a suitable choice of parameters A_2 and m_2 is applied to bonds within the horizon of material points on a pre-existing crack tip. To calibrate A_2 and m_2 for a material, consider a bond $\boldsymbol{\xi}$ normal to the axis of a growing mode-I fatigue crack (Figure 5). Assume that the deformation in the vicinity of the crack tip is constant in the frame of reference of the crack tip. Further assume that the crack grows through a constant distance da/dN in each loading cycle. It follows that the cyclic strain and remaining life this fixed bond $\boldsymbol{\xi}$ may be written in the form

$$\varepsilon(N) = \bar{\varepsilon}(z), \qquad \lambda(N) = \bar{\lambda}(z)$$

where $\bar{\varepsilon}$ and $\bar{\lambda}$ are functions of position relative to the crack tip. Here,

$$z = x - \frac{da}{dN} N \tag{15}$$

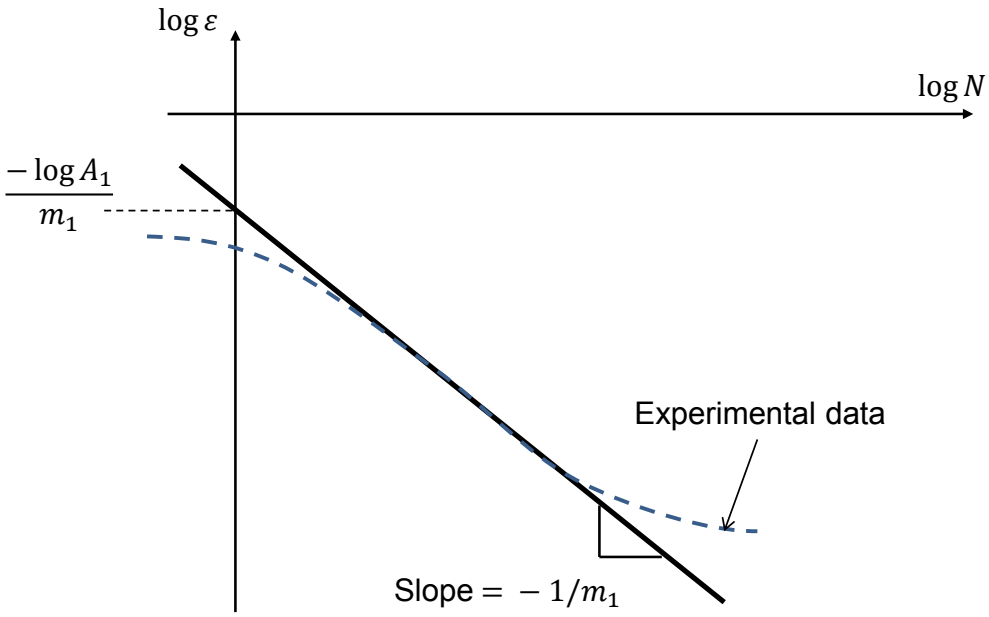

Figure 4. Loading cycles N_1 as a function of bond strain ε_1 for nucleation of damage .

where x is the spatial coordinate along the crack axis chosen such that $z = 0$ for the bond that is on the verge of breaking (that is, the core bond). Compute the remaining life of this bond at $z = 0$ by integrating its first derivative with respect to position:

$$\bar{\lambda}(\delta) = \bar{\lambda}(0) + \int_0^\delta \frac{d\bar{\lambda}}{dz}\, dz.$$

Using the chain rule, this becomes

$$\bar{\lambda}(\delta) = \bar{\lambda}(0) + \int_0^\delta \frac{d\lambda}{dN}\frac{dN}{dz}\, dz.$$

Using (11) and (15) yields

$$\bar{\lambda}(\delta) = \bar{\lambda}(0) + \frac{A_2}{da/dN}\int_0^\delta (\bar{\varepsilon}(z))^{m_2}\, dz. \tag{16}$$

Recall the assumption that in the growth phase, the evolution law (11) applies only to bonds within the horizon of the crack tip, thus

$$\bar{\lambda}(\delta) = 1. \tag{17}$$

From (7) applied to cyclic loading, it follows that

$$\bar{\varepsilon}(z) = \bar{\varepsilon}(0) f(z) \tag{18}$$

where f is a function defined by

$$f(z) = \hat{f}\left(\frac{z}{\delta}\right). \tag{19}$$

Here, $\hat{f}$ is the same function as in Section 3. At the core bond, the remaining life vanishes, because this bond is on the verge of breakage:

$$\bar{\lambda}(0) = 0. \tag{20}$$

Combining (16), (17), (18), and (20) leads to

$$\frac{\beta A_2 (\bar{\varepsilon}(0))^{m_2}}{da/dN} = 1 \tag{21}$$

where

$$\beta = \int_0^\delta (f(z))^{m_2}\, dz. \tag{22}$$

By the definition of the z coordinate, $\bar{\varepsilon}(0) = \varepsilon_{\text{core}}$, yielding a relation between the crack growth rate and the core cyclic bond strain:

$$\frac{da}{dN} = C\varepsilon_{\text{core}}^{m_2}, \qquad C = \beta A_2. \tag{23}$$

Extending the reasoning in Section 3 to cyclic loading, it follows that $\varepsilon_{\text{core}}$ is proportional to the cyclic stress intensity factor ΔK. Also recall the well-known Paris law for fatigue crack growth:

$$\frac{da}{dN} = c\Delta K^M. \tag{24}$$

where c and M are constants. Comparing (23) with (24) leads to the conclusion that the exponents are the same in both expressions, that is,

$$m_2 = M. \tag{25}$$

Therefore, the parameter m_2 may be obtained directly from Paris law data for a material (that is, a plot of $\log(da/dN)$ versus $\log(\Delta K)$).

Because β and $\varepsilon_{\text{core}}$ are unknown, the remaining parameter A_2 cannot be evaluated directly from the data. Instead, a computational model must be run for a single experiment to calibrate A_2. To do this, a computational model of some convenient test is carried out with an arbitrary value for the parameter A_2; call this value A'. Suppose the computational model predicts a crack growth rate $(da/dN)'$, while *real* crack growth rate is da/dN. Then the calibrated value for A_2 in the peridynamic model is given by

$$A_2 = A' \frac{da/dN}{(da/dN)'}.$$

This follows from the linear dependence of da/dN on A_2 in (23).

4.3 Scaling of parameters with the horizon

Suppose the fatigue model parameters m_1, m_2, A_1, and A_2 are known for some value of the horizon δ through the calibration methods discussed previously. The situation frequently arises in peridynamic modeling that the horizon needs to be changed, typically because a different computational grid with more or less resolution is needed for an application. This raises the question of how the fatigue model parameters should change with δ.

First consider the scaling of the nucleation phase parameters A_1 and m_1. Recall from Section 4.1 that these parameters are obtained directly from test data (the S-N curve), so they must be independent of δ.

Next consider the growth phase parameters A_2 and m_2. It is required that da/dN be unchanged as δ is varied. Since m_2 is obtained directly from experimental data (the slope of the Paris law curve), this parameter must be independent of δ. Now recall (23), allowing for dependence of the parameters on δ:

$$\frac{da}{dN} = \beta(\delta)A_2(\delta)(\varepsilon_{\text{core}}(\delta))^{m_2}. \tag{26}$$

From (5) applied to cyclic loading,

$$\varepsilon_{\text{core}}(\delta) = \hat{\varepsilon}_{\text{core}} \frac{\Delta K}{E\sqrt{\delta}} \tag{27}$$

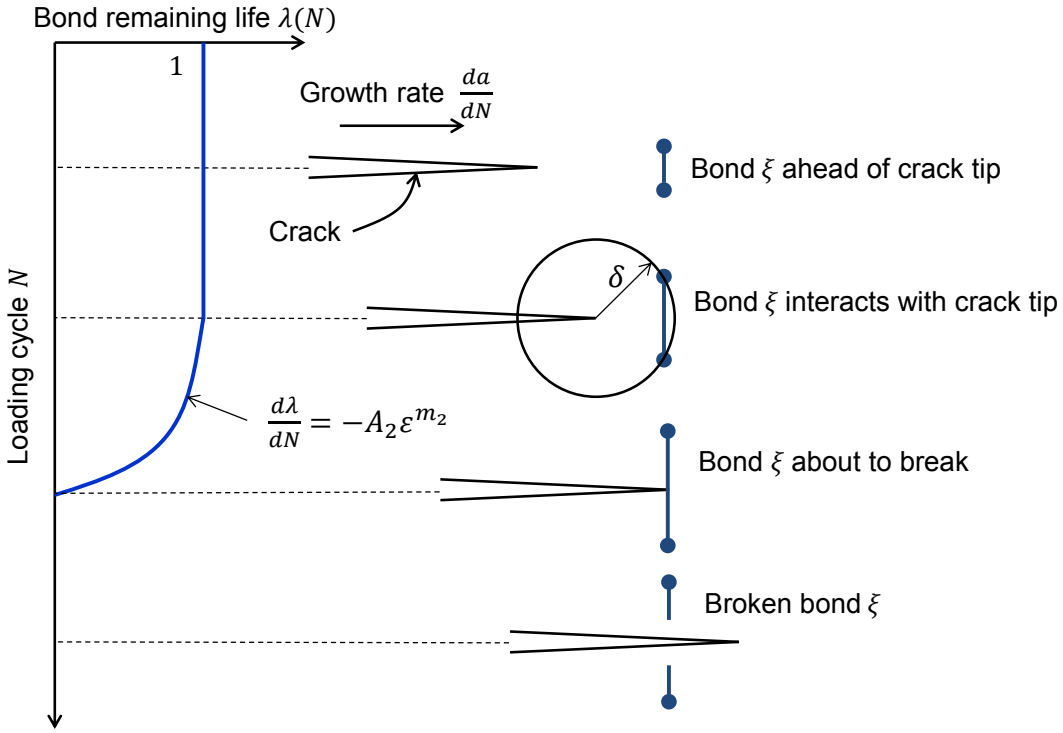

Figure 5. A bond $\boldsymbol{\xi}$ near an approaching fatigue crack undergoes cyclic strain ε, which changes over time, eventually causing the bond to break.

where $\hat{\varepsilon}_{\text{core}}$ is independent of δ, E and the cyclic stress intensity factor ΔK. From (19) and (22), using the change of variables $\hat{z} = z/\delta$,

$$\beta(\delta) = \hat{\beta}\delta, \qquad \hat{\beta} = \int_0^1 (\hat{f}(\hat{z}))^{m_2} d\hat{z}. \tag{28}$$

Note that $\hat{\beta}$ is dimensionless and independent of δ. From (26), (27), and (28),

$$\frac{da}{dN} = \hat{\beta}\delta A_2(\delta) \left(\hat{\varepsilon}_{\text{core}}\delta^{-1/2}\Delta K/E\right)^{m_2}$$

Requiring da/dN to be independent of δ because it is an experimentally measured quantity, it follows that

$$A_2(\delta) = \hat{A}_2\delta^{(m_2-2)/2} \tag{29}$$

where $\hat{A}_2$ is independent of δ.

In summary, when rescaling the horizon for a calibrated set of fatigue model parameters, A_1, m_1 and m_2 are unchanged, while (29) provides the scaling for A_2.

4.4 Transition from phase I to phase II

Although the peridynamic fatigue model has the same basic structure (11) in the nucleation and growth phases, the mechanics of the two phases are different. In the nucleation phase, the peridynamic bond strains are "real," that is, they would agree with a measurement from a strain gauge or DIC applied near the material point $\mathbf{x}$. However, in the growth phase, the bond strains are fictitious because the actual process zone at a crack tip could be much different in size (usually smaller in practice) than our peridynamic continuum-level model. Therefore, the bond strains in a peridynamic model of phase II in general do not correspond to measurable strains. For this reason, the model described in this paper does not smoothly transition between the phases.

In modeling an application in which a fatigue crack nucleates, perhaps at a stress concentration, and then grows to a macroscale crack, we need to specify how the phase I calibration hands off to the phase II. The simplest way to do this in practice is, for a given material particle $\mathbf{x}$, to apply the phase I model until there is some $\mathbf{x}'$ in $\mathcal{H}_{\mathbf{x}}$ with a net damage

$$\phi(\mathbf{x}') \geq 0.5,$$

where ϕ is defined by (4). At that time, we reset the remaining life of bonds connected to $\mathbf{x}$ to 1 and change over to the phase II calibration of the model parameters. An example of a calculation involving both phases is given in Section 5.3.

5 Examples

This section presents computational results for three applications, all involving 7075-T651 aluminum alloy. The first two problems are two-dimensional and illustrate the fitting of the model parameters for the nucleation and growth phases. The third is three-dimensional and demonstrates the ability of the peridynamic model to simulate curved and complex crack trajectories. All calculations used the LPS constitutive model with $E = 70$GPa and $\nu = 0.33$.

All calculations were performed using the discretization described in [28] as implemented in the Emu code [32]. In this method, the equation of motion (1) is approximated by

$$\rho_i \frac{\mathbf{y}_i^{n+1} - 2\mathbf{y}_i^n + \mathbf{y}_i^{n-1}}{\Delta t^2} = \sum_{j \in \mathcal{H}_i} \mathbf{f}(\mathbf{x}_j, \mathbf{x}_i, t^n) \Delta V_j + \mathbf{b}_i^n \qquad \forall \mathbf{x}_i \in \mathcal{B} \tag{30}$$

where i and j are node numbers, ΔV_j is the reference volume of node j, n is the time step number, and Δt is the time step size. For quasi-static problems, dynamic relaxation is applied to damp out kinetic energy. In applying the fatigue model, each bond $\boldsymbol{\xi}_{i,j}$ that connects $\mathbf{x}_i$ to $\mathbf{x}_j$ has a value of remaining life $\lambda_{i,j}^n$ that evolves according to the discetized form of (11):

$$\lambda_{i,j}^0 = 1, \qquad \frac{\lambda_{i,j}^n - \lambda_{i,j}^{n-1}}{\Delta t} = -A(\varepsilon_{i,j}^n)^m$$

where $\varepsilon_{i,j}^n$ is the cyclic bond strain in time step n, and m is the exponent in the power law (11).

The numerical model uses a fictitious simulation time t that is mapped to the current loading cycle N by one of two optional methods (alternative mappings are possible but have not been tested):

- *Linear mapping:*
$$N = t/\tau \tag{31}$$
- *Exponential mapping:*
$$N = e^{t/\tau} \tag{32}$$
where τ is a constant.

In either time mapping, the rate of change of the remaining life of a bond is mapped to the simulation time using the above relations and the chain rule:

$$\frac{d\lambda}{dt} = \frac{d\lambda}{dN}\frac{dN}{dt}$$

where $d\lambda/dN$ is supplied by the power law (11). The linear time mapping (31) is more useful when the number of loading cycles to failure can be estimated in advance. The exponential time mapping (32) is more useful when this is not possible, or in comparing different loading

conditions for which the number of loading cycles to failure varies widely. For example, in reproducing the S-N data discussed in the next section, N varies over eight orders of magnitude, and we wish to avoid computational costs that similarly span eight orders of magnitude. The exponential mapping makes this possible, since the cost is proportional to t rather than N.

The computational model does not explicitly compute cyclic loads on the body. Only the + boundary loading (that is, the more strongly tensile loading condition of the two extreme states + and −) is computed. For a given bond, the resulting strain is s^+. It is assumed, for purposes of these examples, that

$$s^- = Rs^+ \tag{33}$$

where R is the load ratio (the ratio of highest to lowest boundary load). The cyclic strain in the bond is then found from

$$\varepsilon = |s^+ - s^-| = |(1 - R)\varepsilon^+|.$$

5.1 Nucleation at a stress concentration

A two-dimensional model of an hourglass test specimen made of 7075-T651 was used to demonstrate the model parameters for nucleation of fatigue damage (Figure 6). A loading ratio of $R = 0$ was assumed, where $R = \sigma^-/\sigma^+$. The model parameters A_1 and m_1 were evaluated using the calibration procedure described above in Section 4.1, using experimental data of Zhao and Jiang (Figure 7 of [35]). The resulting parameters are listed in Table 1. This table includes values for use with a fatigue limit as discussed below in Section 6.2.

Loading at the ends creates a stress concentration near the midplane of the specimen, leading to the nucleation of damage (Figure 7). The calibrated model results, with and without a fatigue limit, are compared with the test data of Zhao and Jiang [35] in Figure 8.

5.2 Crack growth in a compact test specimen

In this problem, a pre-existing crack is present in a compact test specimen made of 7075-T651 aluminum alloy (Figure 9). Cyclic loads with extremes $P^+ = 1620$N and $P^- = 162$N are applied at the pins, resulting in a load ratio of $R = 0.1$ and a load amplitude of $\Delta P/2$=730N. The growth model parameters were obtained from this problem using the calibration procedure described above in Section 4.2 and the the experimental data of Zhao, Zhang, and Jiang ($R = 0.1$ data in Figure 5 of [36]).

The computed deformation is shown at the start of problem and after extensive crack growth in Figure 10. The crack tip position as a function of the loading cycle is shown in Figure 11 (left). The rate of crack growth accelerates as the crack approaches the free surface because the load is sustained by a thinner and thinner cross-section ahead of the crack as it grows.

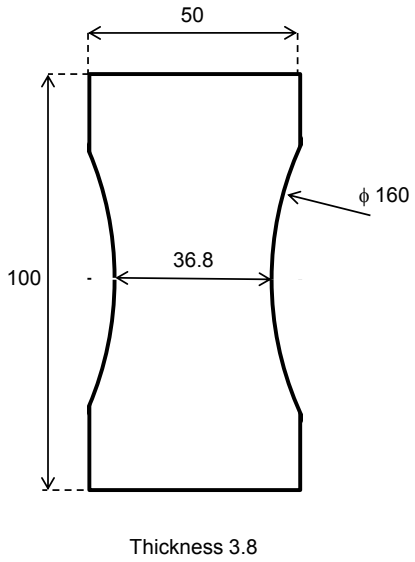

Figure 6. Geometry of the hourglass test specimen modeled in Example 1 (all dimensions are in mm).

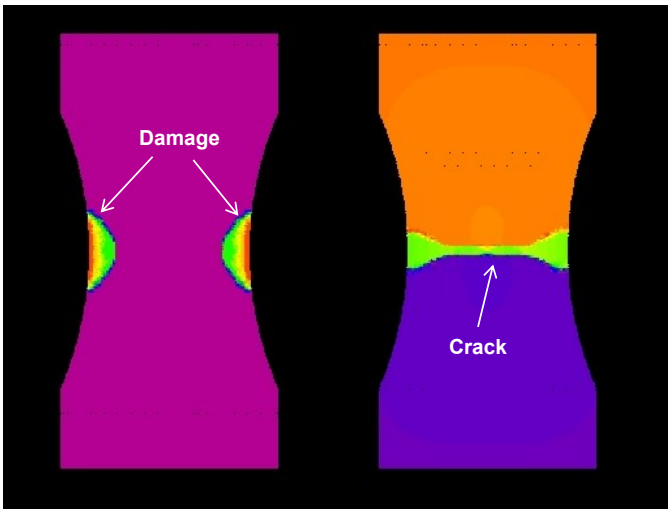

Figure 7. Left: nucleation of fatigue damage in the hourglass test specimen modeled in Example 1. Right: nucleation quickly leads to growth of a crack through the specimen.

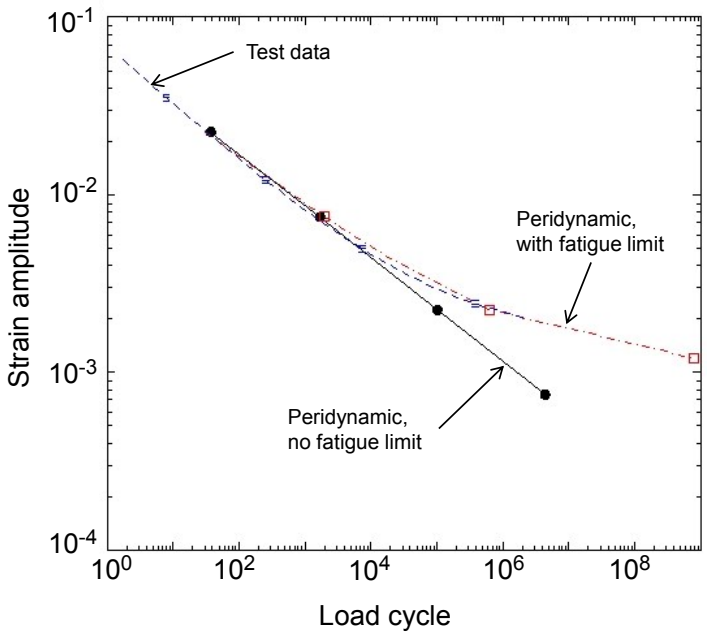

Figure 8. Strain amplitude as a function of loading cycle at which nucleation of damage occurs in the hourglass test specimen modeled in Example 1. Model results are shown with and without a fatigue limit. Experimental data from Zhao and Jiang [35].

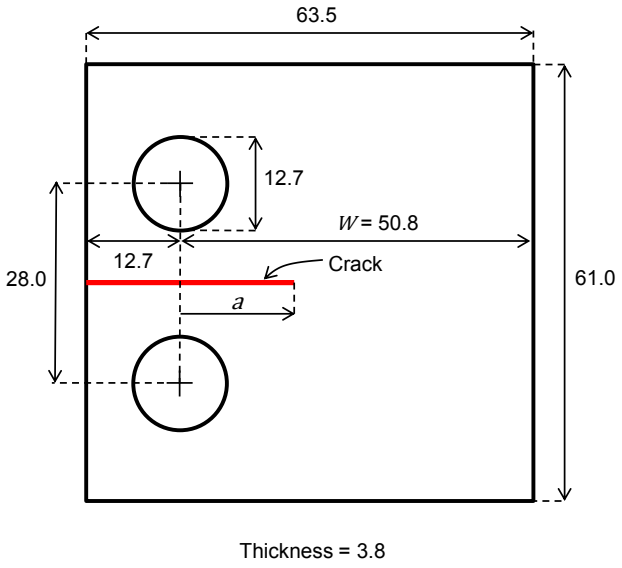

Figure 9. Geometry of the compact test specimen modeled in Example 2 (all dimensions are in mm).

The calibrated model results are compared against the test data from [36] on the Paris law plot in Figure 11 (right). The stress intensity factors, although they are not used in the peridynamic model, were obtained for purposes of calibration using the analytic expression in [36] for this geometry as a function of crack length.

5.3 Torsion of a rod

This example illustrates the nucleation of a fatigue crack at a stress concentration and its growth on a curved trajectory in three dimensions. A 7075-T651 aluminum alloy rod has 50mm length and 20mm diameter. The rod contains a hemispherical cavity 3mm in diameter at the surface, located at the midplane (Figure 12). The ends of the rod are rotated relative to each other in each loading cycle. The rotation angles oscillate between the extreme values 0 and 1°. The problem is modeled with the numerical discretization described in [28] with a

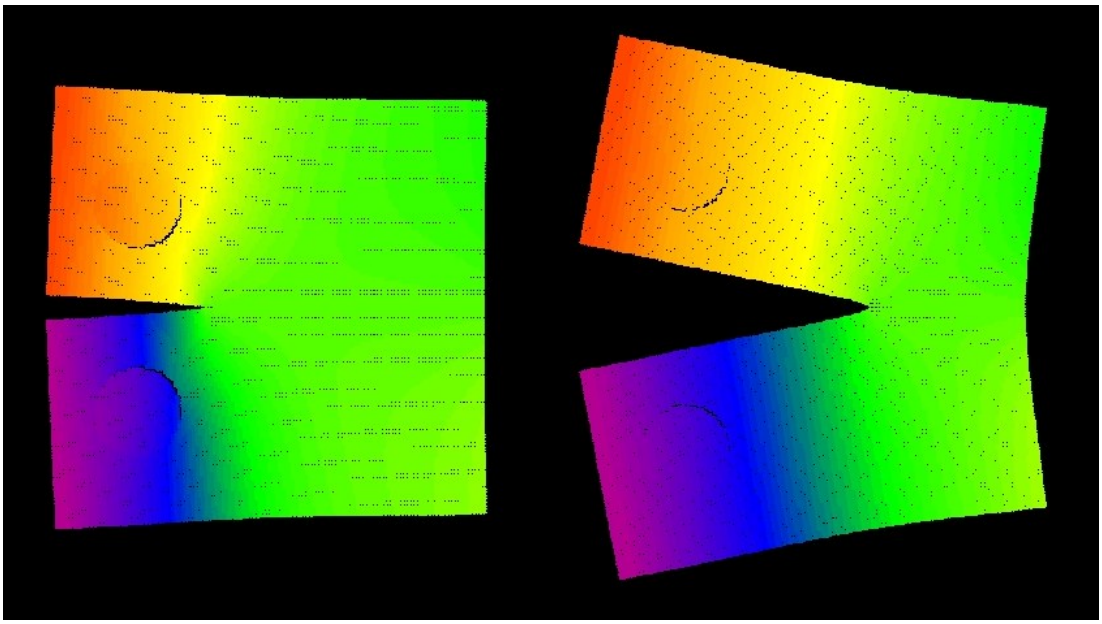

Figure 10. Model results for crack growth in the compact test specimen in Example 2. Left: 0 cycles. Right: 89,000 cycles. Displacements are exaggerated x50. Colors indicate vertical displacement.

Parameter	*Without fatigue limit*	*With fatigue limit*
A_1	1050	2100
A_2	1800	1800
m_1	3.4	3.4
m_2	3.0	3.0
ε_∞	0	0.002

Table 1. Calibrated peridynamic fatigue model parameters for 7075-T651 aluminum alloy for the case $r = \delta = 0.0005$m. See (37) for the form of the model with a fatigue limit.

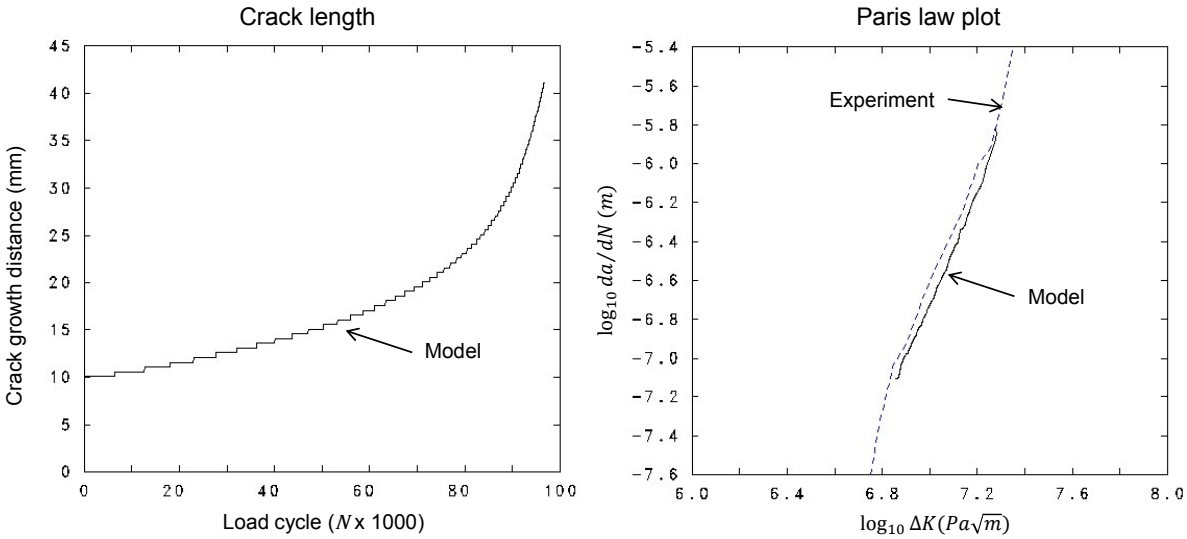

Figure 11. Compact test specimen model results for $R = 0.1$ (Example 3). Left: crack growth distance as a function of loading cycle. Right: Paris law plot, including test data [36].

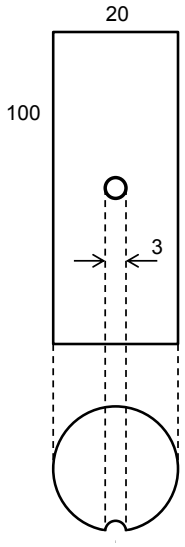

Figure 12. Geometry of the rod modeled in Example 3 (all dimensions are in mm).

grid spacing of approximately 0.5mm.

When the ends of the rod are rotated, a strain concentration occurs near the cavity. This leads to nucleation of fatigue damage at 1.2×10^6 cycles. The damage progresses to growth of fatigue cracks. These cracks grow approximately normal to the direction of maximum tensile stress, leading to a helical trajectory (Figure 13). Helical cracks are commonly observed in rods with a surface defect under torsion [1].

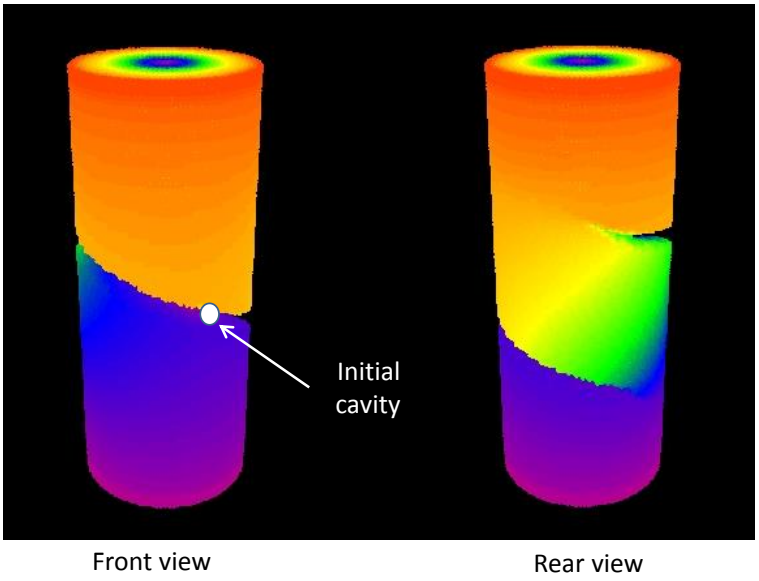

Figure 13. Computed solution for the torsion example problem after 3.5×10^7 cycles. The two views are from opposite sides of the specimen. The white dot shows the location of the initial cavity. Shading indicates magnitude of displacement.

6 Extensions

This section discusses some enhancements to the peridynamic fatigue model for special purposes.

6.1 Loading spectrum

In the development in Section 4, it is assumed that for any bond at any given time, there is a definite value of the cyclic bond strain $\varepsilon(\mathbf{x}, \boldsymbol{\xi})$ (although this value can change as damage evolves or boundary loading changes). However, in many applications, loading occurs over some combination of frequencies. To derive a version of (11) that applies in this case, suppose that the bond strain consists of the superposition of J component angular frequencies ω_j, each with amplitude ε_j:

$$\varepsilon = \sum_{j=1}^{J} \frac{1}{2} \varepsilon_j \cos(\omega_j t).$$

This situation is described approximately by Miner's rule [20, 14], which posits that failure will occur when

$$\sum_{j=1}^{J} \frac{n_j}{N_j} = 1 \tag{34}$$

where n_j is the number of cycles in component frequency ω_j up to the time of failure t_f, and N_j is the number of cycles to failure if ω_j were the *only* component frequency in the loading spectrum. To apply Miner's rule in the peridynamic model, use the definition of frequency and (14) to obtain

$$n_j = \frac{\omega_j t_f}{2\pi}, \qquad N_j = \frac{1}{A \varepsilon_j^m}. \tag{35}$$

Combine (34) and (35) and solve for t_f:

$$t_f = \frac{2\pi}{A \sum_{j=1}^{J} \omega_j \varepsilon_j^m}.$$

Since, in the peridynamic model, λ changes from 1 to 0 over the time interval t_f, we can make the approximation $d\lambda/dt = -1/t_f$. Therefore, the appropriate expression for change in remaining life of a given bond is found to be

$$\lambda(0) = 1, \qquad \frac{d\lambda}{dt} = -\frac{A}{2\pi} \sum_{j=1}^{J} \omega_j \varepsilon_j^m. \tag{36}$$

In comparing this with the single-component expression (11), note that $\lambda(t)$ is now treated as a function of time rather than loading cycle N. In the above expressions, $\{A, m\}$ would be replaced by $\{A_1, m_1\}$ and $\{A_2, m_2\}$ in the nucleation and growth phases of fatigue, respectively.

6.2 Fatigue limit

In some materials, there is no fatigue damage if the loading is less than some lower limit on the S-N curve. To incorporate such a fatigue limit into the peridynamic fatigue model, the nucleation phase in (11) is modified as follows:

$$\lambda(0) = 1, \qquad \frac{d\lambda}{dN}(N) = \begin{cases} -A_1(\varepsilon - \varepsilon_\infty)^{m_1}, & \text{if } \varepsilon > \varepsilon_\infty, \\ 0 & \text{otherwise.} \end{cases} \tag{37}$$

where ε_∞ is the lowest cyclic bond strain that results in damage over a very large number of load cycles. An example of an S-N curve predicted by the peridynamic model with a fatigue limit is shown in Figure 8.

6.3 Phase III

Ultimate failure of a structure due to the uncontrolled growth of a fatigue crack is sometimes called "phase III." Although this is the final culmination of the fatigue process in the failure of engineering components, it is controlled by the mechanics of static, rather than cyclic loading. To treat phase III within the present framework, we can include static fracture parameters as an additional bond failure criterion. Thus, a bond breaks irreversibly when either

$$\lambda(N) \le 0 \qquad \text{or} \qquad s^+ \ge s_*$$

where s_* is the critical bond strain for failure under static loading, as described in Section 2. This critical strain can be calibrated to reproduce K_{Ic} in brittle materials [29].

6.4 Nonzero load ratio

For many materials, the load ratio $R = P^-/P^+$ has a strong effect on the rate of fatigue damage, where P^+ and P^- are the loads applied at the two extremes of the cyclic loading. This effect motivates modification of the Paris law expression (24) to include dependence on R, either explicitly or implicitly. Kujawski [8], and Dinda and Kujawski [5] consider a version of the Paris law in which, in the present notation, the rate of crack growth is given by

$$\frac{da}{dN} = c(K^*)^M, \qquad K^* = (K^+)^\alpha \left(K^+ - \max\{0, K^-\}\right)^{1-\alpha} \tag{38}$$

where c, M, and α are constants, $0 \le \alpha \le 1$, and it is assumed that $K^+ \ge 0$.

To include the effect of load ratio in the peridynamic model, it is sufficient to observe that in an elastic model, the bond strains in the vicinity of a crack tip are proportional to K. Therefore, (11) can be modified in the same way as the Paris law to account for the load ratio. As an example, (38) can be adapted in the form

$$\lambda(0) = 1, \qquad \frac{d\lambda}{dN}(N) = -A_2(\varepsilon^*)^{m_2} \tag{39}$$

where, instead of the cyclic bond strain defined in (10), we have

$$\varepsilon^* = (s^+)^\alpha \left(s^+ - \max\{0, s^-\}\right)^{1-\alpha}$$

and α has the same value as in (38). Even when this modified expression is used, (25) continues to apply.

7 Discussion

The peridynamic fatigue model described here retains the main advantages of the peridynamic theory applied to crack growth: autonomous nucleation and growth of cracks in any direction along complex paths in three dimensions. A key advantage of the model is that the actual loading cycles are not computed explicitly; only the + loading state is computed, with changing patterns of damage inside the body. With the help of the time-to-load cycle mappings discussed in Section 5, very large numbers of load cycles can be computed at reasonable computational cost.

It is possible that future work will reveal the detailed structure of the deformation field near a crack tip in a peridynamic medium, thus providing the form of $\varepsilon_{\text{core}}$ and $\hat{f}$ explicitly. This would allow β to be evaluated from (22), which would permit all four parameters A_1, A_2, m_1, m_2 to be evaluated directly from material test data without simulating the boundary value problem currently needed to find A_2.

The examples in Section 5 used the LPS material model, but the fatigue model itself does not assume any particular material model. It seems possible to apply the fatigue model in conjunction with an elastic-plastic material model, with which it might be possible to study crack closure effects. In this case, it would be necessary to avoid the assumption (33), which implicitly assumes linear elastic material response. Dropping this assumption would then require both the + and − states to be computed everywhere in the body as a function of time, rather than just the + state. This would involve simultaneously modeling the same body twice, with the + and − boundary loads, with the identical damage state in both bodies as time progresses. Fatigue cracks at interfaces between materials can be treated by calibrating the parameters A and m separately for bonds that connect one material to another.

References

[1] M. R. Bache and W. J. Evans. Tension and torsion fatigue testing of a near-alpha titanium alloy. *International Journal of Fatigue*, 14:331–337, 1992.

[2] S. Bordas and B. Moran. Enriched finite elements and level sets for damage tolerance assessment of complex structures. *Engineering Fracture Mechanics*, 73:1176–1201, 2006.

[3] O. K. Chopra. Mechanism and estimation of fatigue crack initiation in austenitic stainless steels in LWR environments. Technical Report NUREG/CR-6787, ANL-01/25, Argonne National Laboratory, 2002.

[4] A. de Andrés, J. L. Pérez, and M. Ortiz. Elastoplastic finite element analysis of three-dimensional fatigue crack growth in aluminum shafts subjected to axial loading. *International Journal of Solids and Structures*, 36:2231–2258, 1999.

[5] S. Dinda and D. Kujawski. Correlation and prediction of fatigue crack growth for different R-ratios using $K_{\max}$ and ΔK^+ parameters. *Engineering Fracture Mechanics*, 71:1779–1790, 2004.

[6] W. Elbert. The significance of fatigue crack closure. In *Damage Tolerance in Aircraft Structures: A Symposium Presented at the Seventy-third Annual Meeting American Society for Testing and Materials, Toronto, Ontario, Canada, 21-26 June 1970*, volume 486, pages 230–242. ASTM International, 1971.

[7] R. Erdogan. Crack propagation theories. Technical Report CR-901, NASA, 1967.

[8] D. Kujawski. A fatigue crack driving force parameter with load ratio effects. *International Journal of Fatigue*, 23:S239–S246, 2001.

[9] H. W. Liu and N. Iino. A mechanical model for fatigue crack propagation. In *Proc. 2nd International Conference on Fracture, Paper 71*, pages 812–823. Chapman-Hall, 1969.

[10] E. Madenci and E. Oterkus. *Peridynamic Theory and Its Applications*. Springer, New York, 2013.

[11] S. Majumdar and J. Morrow. Correlation between fatigue crack propagation and low cycle fatigue properties, ASTM STP 559. In *Fracture Toughness and Slow-Stable Cracking, Part 1*, pages 159–182. ASTM International, 1974.

[12] R. C. McClung and H. Sehitoglu. On the finite element analysis of fatigue crack closure–1. Basic modeling issues. *Engineering Fracture Mechanics*, 33:237–252, 1989.

[13] R. C. McClung and H. Sehitoglu. On the finite element analysis of fatigue crack closure–2. Numerical results. *Engineering Fracture Mechanics*, 33:253–272, 1989.

[14] M. A. Miner. Cumulative damage in fatigue. *Journal of Applied Mechanics*, 12:159–164, 1945.

[15] N. Moës, A. Gravouil, and T. Belytschko. Non-planar 3D crack growth by the extended finite element and level sets–Part I: Mechanical model. *International Journal for Numerical Methods in Engineering*, 53:2549–2568, 2002.

[16] N. Moës, A. Gravouil, and T. Belytschko. Non-planar 3D crack growth by the extended finite element and level sets–Part II: Level set update. *International Journal for Numerical Methods in Engineering*, 53:2569–2586, 2002.

[17] MSC Software Corporation. MSC Fatigue. www.mscsoftware.com.

[18] O. Nguyen, E. A. Repetto, M. Ortiz, and R. A. Radovitzky. A cohesive model of fatigue crack growth. *International Journal of Fracture*, 110:351–369, 2001.

[19] E. Oterkus, I. Guven, and E. Madenci. Fatigue failure model with peridynamic theory. In *IEEE Intersociety Conference on Thermal and Thermomechanical Phenomena in Electronic Systems (ITherm), Las Vegas, NV, June 2010*, pages 1–6, 2010.

[20] A. Palmgren. Die lebensdauer von kugellagern. *Zeitschrift des Vereins Deutscher Ingenieure*, 68(14):339–341, 1924.

[21] P. Paris and F. Erdogan. A critical analysis of crack propagation laws. *Journal of Basic Engineering*, 85:528–533, 1963.

[22] N. Pugno, M. Ciavarella, P. Cornetti, and A. Carpinteri. A generalized Paris' law for fatigue crack growth. *Journal of the Mechanics and Physics of Solids*, 54:1333–1349, 2006.

[23] D. Radaj and M. Vormwald. Elastic-plastic fatigue crack growth. In D. Radaj and M. Vormwald, editors, *Advanced Methods of Fatigue Assessment*, pages 391–481. Springer, New York, 2013.

[24] J. Shi, D. Chopp, J. Lua, N. Sukumar, and T. Belytschko. Abaqus implementation of extended finite element method using a level set representation for three-dimensional fatigue crack growth and life predictions. *Engineering Fracture Mechanics*, 77:2840–2863, 2010.

[25] J. Shi, J. Lua, H. Waisman, P. Liu, T. Belytschko, N. Sukumar, and Y. Liang. X-FEM toolkit for automated crack onset and growth prediction. In *49th AIAA/ASME/ASCE/AHS/ASC Structures, Structural Dynamics, and Materials Conference, Schaumburg, IL, April 2008, Paper AIAA 2008-1763*, 2008.

[26] S. A. Silling. Reformulation of elasticity theory for discontinuities and long-range forces. *Journal of the Mechanics and Physics of Solids*, 48:175–209, 2000.

[27] S. A. Silling. Linearized theory of peridynamic states. *Journal of Elasticity*, 99:85–111, 2010.

[28] S. A. Silling and E. Askari. A meshfree method based on the peridynamic model of solid mechanics. *Computers and Structures*, 83:1526–1535, 2005.

[29] S. A. Silling and E. Askari. A meshfree method based on the peridynamic model of solid mechanics. *Computers and Structures*, 83:1526–1535, 2005.

[30] S. A. Silling, M. Epton, O. Weckner, J. Xu, and E. Askari. Peridynamic states and constitutive modeling. *Journal of Elasticity*, 88:151–184, 2007.

[31] S. A. Silling and R. B. Lehoucq. The peridynamic theory of solid mechanics. *Advances in Applied Mechanics*, 44:73–168, 2010.

[32] Stewart A. Silling. EMU. http://www.sandia.gov/emu/emu.htm.

[33] D. C. Stouffer and J. F. Williams. A model for fatigue crack growth with a variable stress intensity factor. *Engineering Fracture Mechanics*, 11:525–536, 1979.

[34] N. Sukumar, D. L. Chopp, and B. Moran. Extended finite element method and fast marching method for three-dimensional fatigue crack propagation. *Engineering Fracture Mechanics*, 70:29–48, 2003.

[35] T. Zhao and Y. Jiang. Fatigue of 7075-T651 aluminum alloy. *International Journal of Fatigue*, 30:834–849, 2008.

[36] T. Zhao, J. Zhang, and Y. Jiang. A study of fatigue crack growth of 7075-T651 aluminum alloy. *International Journal of Fatigue*, 30:1169–1180, 2008.

DISTRIBUTION:

1	MS 0899	Technical Library, 9536 (electronic copy)
1	MS 0115	OFA/NFE Agreements, 10112

Sandia National Laboratories